

Journal of Materials Chemistry A

Accepted Manuscript



This is an *Accepted Manuscript*, which has been through the Royal Society of Chemistry peer review process and has been accepted for publication.

Accepted Manuscripts are published online shortly after acceptance, before technical editing, formatting and proof reading. Using this free service, authors can make their results available to the community, in citable form, before we publish the edited article. We will replace this *Accepted Manuscript* with the edited and formatted *Advance Article* as soon as it is available.

You can find more information about *Accepted Manuscripts* in the [Information for Authors](#).

Please note that technical editing may introduce minor changes to the text and/or graphics, which may alter content. The journal's standard [Terms & Conditions](#) and the [Ethical guidelines](#) still apply. In no event shall the Royal Society of Chemistry be held responsible for any errors or omissions in this *Accepted Manuscript* or any consequences arising from the use of any information it contains.

Cite this: DOI: 10.1039/c0xx00000x

www.rsc.org/xxxxxx

ARTICLE TYPE

First-Principles Study of O₂ Reduction on BaZr_{1-x}Co_xO₃ Cathode in Protonic-Solid Oxide Fuel Cells

Zhenbin Wang^a, Wenqiang Yang^a, Zhuoying Zhu^a, Ranran Peng^{a,c}, Xiaojun Wu^{a,b,c}, Changrong Xia^a and Yalin Lu^{a,b,c}

Received (in XXX, XXX) Xth XXXXXXXXX 20XX, Accepted Xth XXXXXXXXX 20XX

DOI: 10.1039/b000000x

Bulk proton mobility and catalytic activity to surface oxygen reduction are the two factors to determine the effectiveness of cathode materials for protonic-solid oxide fuel cells (p-SOFCs). In this work, a mixed protonic/electronic conductor (MPEC) of BaZr_{0.75}Co_{0.25}O₃ (BZCO) was selected as a potential cathode for p-SOFCs, and its bulk proton transporting and oxygen reduction behaviours at the microscopic level were investigated using the first-principles approach. Two plausible proton migration pathways in BZCO were examined and the highest proton migration barrier calculated is 0.63 eV, which agrees remarkably well with experimental findings. Compared with the weak adsorption of oxygen on BaZrO₃(100) surface, the BZCO(100) surface provides a relative large adsorption energy of -0.64 eV, indicating that the Co doping enhances the oxygen adsorption on the surface. Furthermore, oxygen reduction reaction over the MPEC cathode surface was explored using a hydrogenated BZCO(100) surface model, where 4 protons are located to react with one O₂ molecule to generate two water molecules. For the formation and desorption of the first water molecule on the BZCO surface, four possible reaction pathways have been mapped out. The potential energy profiles indicate that the reaction with two protons simultaneously migrating to the adsorbed oxygen molecule to break the O-O bond (path-4) is the most feasible process for the formation of the first water molecule. Our study for the first time presents an atomistic level understanding of oxygen reduction and proton migration over or inside the MPEC cathode.

1 Introduction

That to achieve high energy conversion efficiency has been constantly pursued in developing various fuel-cell technologies, in which a prime example is the solid oxide fuel cells (SOFCs).^{1,2} Reducing SOFCs' operating temperature to the intermediate temperature level, say the 500-750 °C range, is one of the major objectives in order to reduce the stack cost and to improve the stack stability. However, at lower operation temperatures, the polarization resistance, generally from the electrochemical reactions occurring at the cathode side, increases sharply and becomes a major source for cell resistance, which greatly depresses the SOFCs' power output. Most importantly, the performance loss of a SOFC is mainly due to the sluggish O₂ reduction reaction on the cathode surface at lower temperatures.^{3,4} To ameliorate the cathode reaction efficiency, it is indeed a key to understand the underlying of O₂ reduction at the cathode.

Recently, proton-conducting solid oxide fuel cells (p-SOFCs), with relative lower activation energies for proton transporting with respect to the traditional oxygen-ion conducting SOFCs (O-SOFCs), have gained much attention in the striving for efficient intermediate temperature SOFCs.^{5,6} Their much lowered activation energies are advantageous for the electrode (especially

cathode) reaction at intermediate temperatures.

Numerous experimental attempts have been previously made to probe the oxygen reduction mechanism of the cathode materials. He *et al.* developed a cathode reaction model for p-SOFCs and examined the rate-determining step of the cathode reaction with respect to both oxygen and water vapour partial pressures.⁷ It is believed that the limiting steps of the cathode reactions for p-SOFCs involve the proton transporting to triple phase boundaries (TPBs), and the oxygen catalytic dissociating and then transporting to the TPBs when using either electronic conducting cathodes or composite cathodes composed of proton conductors and oxygen ion-electron mixed conductors, such as Pt⁸, BaCe_{0.8}Sm_{0.2}O_{3-δ}-Sm_{0.5}Sr_{0.5}CoO_{3-δ}⁷ and Ba(Zr_{0.1}Ce_{0.7}Y_{0.2})O_{3-δ} (BZCY)-La_{0.6}Sr_{0.4}Co_{0.2}Fe_{0.8}O_{3-δ} (LSCF)⁹, *et al.* That is to say, the cathode reaction for p-SOFCs is more complicated than that for O-SOFCs due to that in the latter case only oxygen dissociation and transporting processes are required. Nevertheless, little investigation at the microscopic level has been done so far to fundamentally understand the detailed reaction processes over the cathode for p-SOFCs.

Interestingly, much effort has been devoted to theoretically understanding the oxygen reduction and transporting for O-SOFCs by using the density functional theory method in recent

years. Choi *et al.* studied the O₂ reduction on LaMnO₃ and La_{1-x}Sr_xMnO₃ (LSM) surfaces and found that Mn species are more active than La and Sr for the O₂ reduction, and that the adsorption and dissociation reactions are barrierless.^{10,11} Moreover, Mastrikov *et al.* proposed that the encountering of O⁻ with surface oxygen vacancy is the rate-determine step for the O₂ reduction on the LSM cathode based on *ab initio* thermodynamics analysis.^{12,13} Very recently, we explored oxygen bulk transporting properties and O₂ reduction on La_{1-x}Sr_xCo_{1-y}Fe_yO₃ cathodes and predicted that the dissociated oxygen prefers to diffuse along the surface rather than through the bulk cathode and that Co species, compared with Fe species, help to reduce the oxygen vacancy formation energy and therefore facilitate the oxygen ion transporting.¹⁴ In fact, the first-principles calculations have provided an unprecedented insight into the bulk oxygen transporting and oxygen reduction over the cathode surfaces.

To design a novel and high efficient cathode for p-SOFCs, a microscopic level understanding of the cathodic processes, involving proton migration, O₂ adsorption and reduction, and water formation and desorption, will be very consequential. In this work, we investigated the O₂ reduction on a MPEC cathode material of Co-doped BaZrO₃. Its electronic conductivity, bulk proton transporting properties, as well as the O₂ reduction processes with and without the presence of protons were investigated. In addition, the oxygen bulk mobility of BaZr_{1-x}Co_xO₃ was also examined to evaluate its performance as an O-SOFCs cathode.

2. Computational methods

All calculations were performed using the Vienna *ab initio* simulation package (VASP) with the projector augmented wave (PAW) method.¹⁵⁻¹⁷ The exchange-correlation interaction was described by the generalized gradient approximation (GGA) Perdew-Burke-Ernzerhof(PBE) functional.¹⁸ The plane wave basis set was 480 eV and the electronic energy convergence was set to 10⁻⁵ eV. Structural optimization was carried out until the Hellmann-Feynman force on each atom was smaller than 0.03 eV/Å. This value was selected simply due to that more stringent convergence criterion (e.g. 0.01 eV/Å) gave no change to O₂ adsorption energies and oxygen dissociation barriers. The parameters used in this study ensured a convergence of the total electronic energy within 2 meV per atom. All calculations were spin-polarized.

Integration over the first Brillouin-zone based on the Monkhorst-Pack scheme¹⁹ was performed using a 6×6×6 k-point grid for the five-atom primitive cell. The bulk proton transporting property of BaZr_{1-x}Co_xO₃ was modelled using a 2×2×2 supercell with the number of k points reduced accordingly. The 2x2 slab model with a 4-layer was correspondingly constructed to serve as the surface model to study the oxygen reduction reaction (ORR) on the BaZr_{1-x}Co_xO₃(100) (x = 0, 0.25) surfaces. Here the BaZr_{1-x}Co_xO₃(100) surface was chosen because it was generally believed that the (100) surface was the most stable surface in ABO₃ perovskites.^{10,11} We also calculated the surface energies of BaZr_{1-x}Co_xO₃ with low-index surfaces of (100), (110) and (111) to examine the surface stability. As illustrated in Table S1 (see

ESI† for additional details), the (100) surface offered the smallest surface energy, implying that it might be the most energetically stabilized surface, which is in good consistence with the previous studies.¹¹ Furthermore, our convergence tests showed that variations in the evaluated energies of O₂ adsorption on the BaZr_{1-x}Co_xO₃(100) surface for a thicker slab (six-layer) were insignificant (smaller than 0.02 eV). Thus, a 4-layer slab of the BaZr_{1-x}Co_xO₃ (100) surface was considered to be sufficient for our studies here. The bottom two layers were fixed at the estimated bulk lattice constant, while the rest were allowed to relax freely. A vacuum spacing of 15 Å was placed in the direction perpendicular to the surface. Compared with those using 15 Å, a larger vacuum gap, e.g. 20 Å, gave no changes to adsorption energies of O₂ on the BaZr_{1-x}Co_xO₃(100) surface. Additionally, to avoid the fictitious dipole moment (weak polarity²⁰), dipole corrections were applied in all calculations of surfaces. The climbing image nudged elastic band (CI-NEB) method²¹ was employed to locate the minimum energy paths (MEPs) and the transition states for the oxygen reductions on the BaZr_{1-x}Co_xO₃ cathodes. In order to analyse the charge transferring, effective charges of atoms in BZCO were estimated using the Bader method^{22,23}. As depicted in Table S2, effective charge of Ba atom (1.55±0.01e) was close to its normal charge of +2e, whereas charges of B site atoms (Zr, Co) were much smaller than their normal charges of +4e, and charges on O atom was also prominently reduced if comparing to its normal charge of -2e. The significant difference between the effective charges of B sites atoms and O atom and their normal charges might result from the exceptionally pronounced covalency of the B-O chemical bonding in the perovskites.^{12,13}

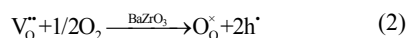
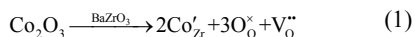
The DFT+U method has been considered more desirable to predict the electronic structures inside the strongly correlated materials, especially for their magnetic properties at the low temperature.^{24,25} We therefore performed a test calculation using the DFT+U method on the migration barrier and the surface adsorption inside/over the BZCO cathode to verify the DFT calculation. The highest oxygen migration barrier in BZCO, calculated using the DFT+U approach, was 1.13 eV, close to the standard DFT estimation of 1.21 eV. Meanwhile, the highest proton migration barrier along the [010] direction, was 0.62 eV using the DFT+U approach, also similar to the standard DFT value of 0.53 eV. Agreement of the migration barrier calculated using both DFT+U and DFT methods suggested that the DFT was also feasible to predict the migration barrier in our BZCO sample. Nevertheless, based on the *Co-top-2* adsorption structure (see Fig.4), the estimated adsorption energy of O₂ on the BZCO(100) surface was 0.17 eV using the DFT+U (U = 3.3²⁶) approach, whereas this value with the DFT strategy was -0.46 eV. The positive value of the adsorption energy calculated using the DFT+U method meant the adsorption process was exothermic, implying that this process was impossible to take place at 0K. This was obviously absurd^{10-14,27-29}, suggesting that the DFT+U method was not feasible to predict the surface reaction. And therefore, we neglected the U effect in this report, similar to those previous reports^{10-14, 27-29}.

3. Results and discussion

3.1 Geometry and electronic structures of $\text{BaZr}_{1-x}\text{Co}_x\text{O}_3$ ($x = 0, 0.25$)

BaZrO_3 (BZO) with a cubic structure (space group Pm-3m), as displayed in Fig. 1(a), was adopted for the calculations. The optimized bulk lattice parameter of BZO is 4.247 Å, agreeing well with the experimental value of 4.188 Å³⁰ and the theoretical value of 4.250 Å³¹ too. To simplify the calculations, a compound of $\text{BaZr}_{0.75}\text{Co}_{0.25}\text{O}_3$ (BZCO) was used to model the Co-doped BaZrO_3 cathode. Three possible atomic structures of BZCO were considered for the 2x2x2 supercell, as depicted in Fig. 1(b)-(d). Total electronic energy calculations indicate that the configuration with two Co atoms next to each other is the most energetically stable structure (Fig. 1(b), which was further adopted for the following bulk transporting and surface reaction calculations. Note that its ferromagnetic (FM) state is energetically favourable than the antiferromagnetic (AFM) state with an energy difference of 27 meV per supercell, we then set BZCO at its FM state for all subsequent calculations.

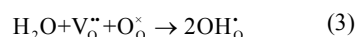
With Co doped into BaZrO_3 , the electron hole (h^*) and the oxygen vacancy could be created to maintain the electro-neutrality, as explained by the following equations using Kroger-Vink notations:



This means that $\text{BaZr}_{0.75}\text{Co}_{0.25}\text{O}_3$ might have considerable electronic (electron hole) conductivity. With the incorporation of an oxygen vacancy into perfect BZCO bulk, effective charge of the Co atoms reduces from the average 1.45 to 1.19 e, as shown in Table S2, indicating the reduction of Co oxidation states at the presence of oxygen vacancy. Here, we calculated the electronic density of state (DOS) of both BZCO and BZO, as displayed in Fig. 2. As shown in Fig. 2 (b), BZO is an insulator with a wide energy band gap of 3.0 eV, in consistent with previously reported theoretical values of 3.0 eV (GGA-PW91)³¹ and 2.6 eV (LDA)³². It is well known that the standard DFT functional will always underestimate the band gap, which makes our value smaller than the experimental value (5.3 eV).^{33,34} In any cases, the insulator property of the pristine BZO means that it is not suitable as a cathode material in SOFCs. With the Co doping, however, the BZCO exhibits metallic characteristics, which facilitates the electron conduction. This feature suggests that BZCO could be a good electronic conductor, which corresponds well with our previous experimental observations.³⁵ Meanwhile, 3d electrons of the Co dopant arise significantly around the Fermi energy level and hybridize with the O 2p electrons, implying an improvement in the charge carrier concentration.³⁶ All these situations are propitious to the electronic conduction. Moreover, the DFT+U method is also used to verify the electronic DOS of BZCO, as illustrated in Fig. S1. The results of the DFT+U intensively indicate the improved electronic conducting behaviours in BZO with Co doping.

3.2 Proton bulk transporting properties in the cathode of $\text{BaZr}_{1-x}\text{Co}_x\text{O}_3$ ($x = 0, 0.25$)

Oxygen vacancies formed with the Co doping (as shown in Eq. (1)) might also lead to a generation of protons in the moist atmosphere, as shown in eq. (3).



Proton transferring was experimentally confirmed as one of the rate limiting steps for p-SOFCs, and therefore, fast proton transporting in the bulk cathode could facilitate an active cathodic reaction process. In doped perovskites, proton migration is generally believed to occur via the two-step Gröthuss diffusion mechanism, which involves the proton reorientation of the hydroxide ion at the oxygen site and the proton transferring between adjacent oxygen ions.³⁷ Both experimental^{6,38} and theoretical³⁹⁻⁴¹ results have verified the influence of dopants on the proton conduction in these perovskites with a proton trapping effect arising from interactions between the dopant ions and the protonic defects. This discovery implies that the proton is prone to diffuse along the dopant because of dopant-defect association (trapping). In the following study, we further explore the potential energy profiles for proton migration between adjacent oxygen sites in the BZCO cathode.

Two representative proton diffusion pathways (in the vicinity of the Co dopant) were mapped out to examine the proton mobility in the BZCO cathode. Fig. 3 (a) and (b) illustrate the proton migrating processes along [010] and [100] directions via rotation (R) and transfer (T) approach, respectively. An overall proton migration pathway along the [010] direction can be summarized as the following process: T12 → R2 → R2 → T21 → T12. The migration barriers of proton involving in these processes were summarized in Table 1a. We found that T12 process offers the highest migration barrier of 0.53 eV and T21 process has the lowest migration barrier of 0.03 eV. We attribute this noticeable difference to the trapping effect of the dopant (Co) to proton transferring, a defect association in fact. And therefore, the process of proton migrating away from O1 to O2 (T12) suffers from the trapping effect of the dopants whereas that proton diffusing from O2 to O1 (T21) benefits from the attraction of the dopants. Fig. 3b shows the process for proton diffusing via R1 → T12 → T23 → R3 → R3 → T32 → T21 → R1 to fulfil a periodic migration along the [100] direction. The migration energies for those pathways were summarized in Table 1(b), and T23 gives the highest migration energy barrier of 0.63 eV. Along the [010] direction, the highest migration energy barrier of proton is about 0.1 eV lower than that along the [100] direction, suggesting that the proton diffusing along the Co-O-Co chain ([010] direction) might be more dominant than that along the Co-O-Zr chain ([100] direction). The calculated migration energy barriers along both [010] and [100] directions agree remarkably well with the experimental values (ranging from 0.45 to 0.65 eV).^{1,2}

Reason for protons transferring along the Co-O-Co chain was also discussed here. As shown in Table S2, when introducing a proton defect into the perfect BZCO bulk, effective charge of Co atoms reduces from the average 1.47 to 1.34 e, while that of Zr atoms remain unchanged. Compared with the large effective

charge of Zr atom (2.21e), the less positive effective charge of Co seems to provide a less repulsion to protons with a positive charge (0.55e). This might be the reason for the optimised path for protons transferring along the Co-O-Co chain, similar to the called association of defects³⁹⁻⁴¹.

For comparison, the proton migration barrier of un-doped BZO was also studied in order to evaluate the Co doping effect on the proton conductivity of BZCO. As shown in Fig. S1, the calculated migration energy barriers of proton between two adjacent oxygen sites in BZO is 0.14 eV (R) and 0.29 eV (T), which is consistent with the reported DFT-PW91-NEB results of 0.14 eV (R) and 0.25 eV (T)⁴², and within the large range of 0.83 ± 0.65 eV in previous quantum molecular dynamic simulations⁴³. The calculated migration barriers in BZO are close to previously reported experimental findings⁶, where the activation energy of the proton diffusion in the association-free region of Y-doped BZO was found to be 0.17 eV.

As our previous experimental work suggested, the BZCO cathode exhibits both oxygen ionic and electronic conducting behaviours under the dry atmosphere, implying that BZCO might be a cathode candidate for O-SOFCs.³⁵ Therefore, we further investigated the oxygen bulk transporting properties of $\text{BaZr}_{1-x}\text{Co}_x\text{O}_3$ ($x = 0, 0.25$) under the dry atmosphere (see S3.2 for additional details). In stark contrast to the small migration barrier of the proton in $\text{BaZr}_{1-x}\text{Co}_x\text{O}_3$ ($x = 0, 0.25$) cathode, the calculated migration energy barrier of oxygen ion is quite large (the highest energy barrier is 1.21 eV in the transporting pathway, refer to Table S2 in the supporting information). This result indicates that the bulk transporting of oxygen ions is sluggish, consisting with our previously reported experimental findings³⁵. Nevertheless, the formation of oxygen vacancy has a significant impact on the proton conductivity by modulating the proton concentration in BZCO. For instance, in BZO, due to its high formation energy (6.39 eV, referring to Table S3), the oxygen vacancy concentration is rather low even under the normal SOFCs operation conditions ($T = 1000$ K, for example). As a result, the proton concentration in BZO is quite low when treated in water vapour, leading to a rather low proton conductivity⁴⁴ and in consequence, evidencing that BZO is not suitable for practical applications even though it embraces a small proton migration barrier. On the contrary, doping two aliovalent Co atoms in BZO, *i.e.* BZCO, induces the oxygen vacancies, and this subsequently enhances the proton concentration when BZCO was exposed to the moist atmosphere. Moreover, it should be pointed out that the proton trapping will be created by the dopant at the same time.

3.3 O₂ adsorption on the surface of $\text{BaZr}_{1-x}\text{Co}_x\text{O}_3$ ($x = 0, 0.25$) cathode

Cathodic reactions in O-SOFCs are generally deemed involving the following processes :1) oxygen initially adsorbs, dissociates and incorporates into the cathode; 2) and then the dissociated oxygen ions diffuse through the bulk or along the surface of the cathode to the electrolyte, as illustrated by Fig. S3. For the oxygen ionic and electronic mixed conducting properties of BZCO in the dry atmosphere, we first examined the O₂ adsorption and dissociation behaviours on the $\text{BaZr}_{1-x}\text{Co}_x\text{O}_3$ ($x =$

0, 0.25)(100) in order to evaluate its effectiveness as a cathode for O-SOFCs.

CoO-terminated BZCO(100) surface was selected to examine the O₂ reduction since it offers the lowest surface energy (see Table S1). Furthermore, the oxygen vacancy located between the two Co atoms requires the smallest energy (0.61 eV) for the formation, comparing to those with Co-O_{vac}-Zr (1.16 eV) and Zr-O_{vac}-Zr (2.72 eV). Three adsorption sites existing on the CoO-terminated BZCO (100) surface were studied, including Co-top, Zr-top and O_{vac}-top. As depicted in Fig. 4, the configuration of O₂ adsorption on the surface oxygen vacancy defect gives the largest adsorption energy of -0.64 eV, which can be ascribed to the Co's doping effect. Accordingly, the O₂ adsorption will inevitably increase the oxidation states of Co atoms, as shown in Table S2. For the comparison purpose, we also calculated the O₂ adsorption on the BZO(100) surface and found that O₂ can't adsorb on it, confirming that the Co doping will enhance the O₂ adsorption on the BZCO cathode surface. Regarding to the dissociation process of O₂ on the BZCO(100) surface, only the most energetically stable adsorption structure (Vac-O₂, in Fig. 4(a)) was considered as the initial structure. Thus, after it stably adsorbed on the BZCO(100) surface, the O₂ molecule decomposed into two monoatomic oxygen species, one incorporating into an oxygen vacancy and the other diffusing to a more energetically stable site (Co-diss) with an energy barrier of 1.15 eV. This rather high dissociation barrier evidences the relative sluggish reduction behaviour and, on the contrary, proves the higher efficiency (*vide infra*) of the BZCO cathode in O₂ reduction under the wet atmosphere.

3.4 O₂ reduction on the surface of BZCO cathode in wet atmosphere

For p-SOFCs, it was suggested that the cathodic reactions over a MPEC cathode involve the following steps: 1) protons migrate from the electrolyte to the cathode and then transport from the cathode bulk to surface, as illustrated in Fig. 5; 2) oxygen molecules from the surrounding atmosphere adsorb on the MPEC cathode surface, dissociate and then react with electrons and protons to form water; 3) finally, the formed water molecules escape from the cathode surface to the gas phase.

In order to disclose the O₂ reduction mechanism on the MPEC cathode, a hydrogenated BZCO(100) surface with 4 proton defects and one O₂ adsorbed on the surface oxygen vacancy was employed, as shown in Fig. 6a-①, where two water molecule would be expected to be generated one after the other. For the formation of the first water molecule, four plausible reaction pathways were mapped out to explicate the O₂ reduction reaction over the BZCO cathode, as depicted in Fig. 6a. For path-1 (olive line), one proton (from left side in the figure) diffuses to the adsorbed O₂ molecule and forms a hydroxyl (②) by overcoming an ignorable energy barrier of 0.02 eV (TS-2). This process is exothermic, releasing energy of 1.77 eV. The second proton (the left side in the same figure) attaches to the hydroxyl to form an adsorbed water molecule (③) with an energy barrier of 0.05 eV (TS-4). Finally, the formed water molecule is released from the BZCO(100) cathode surface (④) to gas phase with an adsorption

heat of 0.80 eV. For path-2 (black line), the oxygen dissociation and the water formation process are the same as those in path-1. While in path-2, the third proton (from the right side in the picture) attaches to the left oxygen ion at first to form a new hydroxyl at the surface oxygen vacancy (⑤) by overcoming an energy barrier of 0.16 eV (TS-5) and releases a heat of 0.37 eV. Then, the preformed water molecule escapes from the surface with an adsorption heat of 0.55 eV (⑦). Compared to that in the path-1, this process releases a heat of 2.14 eV, which is more favourable in energy.

In path-3 (red line), one proton attaches to the adsorbed O₂ and breaks the O-O bond by overcoming an energy barriers of 0.02 eV (TS-1). Before the formation of water molecule, the second proton from the opposite side of hydroxyl transfers to the dissociated oxygen ion to form another hydroxyl with an energy barrier of 0.13 eV (TS-3). Heat of 2.31 eV is released in the forming processes of two adsorbed hydroxyls. Subsequently, one water molecule forms with the third proton jumping to a hydroxyl (⑤) and then desorbs to the atmosphere (⑦) with the adsorption heat of 0.17 and 0.55 eV, respectively. While for path-4 (blue line), two protons from both sides attach synchronously to the adsorbed O₂ molecule by overcoming an energy barrier of 0.06 eV and simultaneously form two hydroxyls with a heat releasing of 2.31 eV. The following water formation process and releasing process is the same as that in path-3 with the endothermic heat of 0.17 and 0.55 eV, respectively. Within the four studied reaction pathways, the O₂ reduction in the path-4 is the most feasible in the light of energy comparison, which only requires overcoming one energy barrier of 0.06 eV to form two hydroxyls, and adsorbing heats of 0.17 and 0.55 eV to form and to release the water molecule. The whole process releases total heat of 2.31 eV. This result also indicates that presence of protons is beneficial to oxygen dissociation process.

Finally, the reduction process of the left oxygen ion was considered. As depicted in Fig. 6a and b, the left structure after releasing the first water molecule through path-1 (⑧) is energetically unstable compared with those (⑨) through path-2-4. Moreover, the thermodynamically stable hydroxyl structure could be formed with the third proton attaches to the left oxygen ion by overcoming an energy barrier of 0.13 eV (TS-6). The second water molecule is subsequently generated with the forth proton attaches to the formed hydroxyl with an energy barrier of 0.90 eV (TS-7). It should be noted that the direct formation of the second water (⑩) from the adsorbed oxygen ion (⑧) is not observed through our calculation process. Desorption of the second water molecule from surface to atmosphere demands to adsorb a heat of 0.60 eV. Compared with the formation and releasing energy of the first water molecule, the formation and releasing of the second water molecule is endothermic, and especially its energy barrier is higher than that in the formation of the first water molecule. Nevertheless, taking an overall of the whole reaction, the O₂ reduction on the BZCO surface with the formation two water molecules per O₂ molecule is exothermic and energetically feasible.

4. Conclusions

In conclusion, a comprehensive first-principles study of O₂ reduction on a single-phase mixed proton and electron conducting (BZCO) cathode in p-SOFCs have been performed. We found that BZCO presents a good electronic conductivity, in contrast to the insulator characteristics of the pristine BZO. The calculated DOS indicates that the enhanced electronic conductivity of BZCO arises from coupling of dopant Co's 3d orbitals and O's 2p orbitals around the Fermi level. Two most plausible bulk transporting pathways of protons in BZCO were mapped. The calculated migration barriers show that the proton diffusing along the Co-O-Zr chain ([100] direction) would provide the largest migration barrier of 0.63 eV, agreeing well with the previous experimental findings. The high oxygen vacancy formation energy (6.39 eV) indicates the inappropriateness of using BZO as a proton conductor even though it enjoys lower proton migration barriers. On the contrary, the smaller formation energy of an oxygen vacancy (0.81 ~ 2.58 eV) in BZCO facilitates the water incorporation by providing more defect locations, and as a consequence, ameliorates the proton concentration. Compared with the pristine BZO surface, O₂ adsorption on the BZCO surface is much enhanced due to the Co doping effect, whereas O₂ dissociation on this surface is found to be sluggish with an energy barrier of 1.15 eV. At last, the O₂ reduction processes were fully examined on the hydrogenated BZCO(100) surface. The most favourable reaction pathway involves the following steps of 1) migration of two protons to the adsorbed O₂ to form two hydroxyls; 2) the first water molecule forms with the third proton transfer to one hydroxyls and then desorbs to the gas phase; 3) the second water molecule forms with the forth proton attached to left hydroxyls and then desorbs to the gas phase. The calculated reaction heat and reaction energy barriers indicate that the O₂ reduction with two water molecules formed per O₂ molecule is feasible in energy. Our results clearly demonstrated that BZCO is a promising material for mixed protonic/electronic conducting cathode applications in p-SOFCs. This microscopic understanding also allowed us to address the pressing problem in minimizing the cathode polarization in p-SOFCs.

Acknowledgements

This work was financially supported by the National Basic Research Program of China (973 Program, 2012CB922001 and 2012CB215403 and 2011CB921400), the NSFC (Grant Nos. 51072193, 21121003), Fundamental Research Funds for the Central Universities (WK2060140014, WK2060190025), and the One Hundred Person Project of CAS. The authors acknowledge Supercomputing Center of USTC and National Supercomputing Center in Tianjin for providing computational resources. Figures with geometry are produced by Jmol [Jmol: an open-source Java viewer for chemical structures in 3D. <http://www.jmol.org/>] and VESTA⁴⁵.

Notes and references

- ^a CAS Key Laboratory of Materials for Energy Conversion, Department of Materials Science and Engineering, University of Science and Technology of China, Hefei, 230026, P. R. China. Fax: 86 551 63600594; Tel: 86 551 63600594; E-mail: pengrr@ustc.edu.cn
- ^b Hefei National Laboratory of Physical Science at the Microscale. Fax: 86 551 63607915; Tel: 86 551 63607915; E-mail: xjwu@ustc.edu.cn

^c Synergetic Innovation Center of Quantum Information & Quantum Physics, University of Science and Technology of China, Hefei, Anhui 230026, China.

[‡] Footnotes should appear here. These might include comments relevant to but not central to the matter under discussion, limited experimental and spectral data, and crystallographic data.

1. E. Fabbri, L. Bi, D. Pergolesi and E. Traversa, *Adv. Mater.*, 2012, **24**, 195-208.
2. E. Fabbri, D. Pergolesi and E. Traversa, *Chem.Soc. Rev.*, 2010, **39**, 4355-4369.
3. S. B. Adler, *Chem. Rev.*, 2004, **104**, 4791-4843.
4. S. B. Adler, *Solid State Ionics*, 1998, **111**, 125-134.
5. K. D. Kreuer, *Annu. Rev. Mater. Res.*, 2003, **33**, 333-359.
6. Y. Yamazaki, F. Blanc, Y. Okuyama, L. Buannic, J. C. Lucio-Vega, C. P. Grey and S. M. Haile, *Nat. Mater.*, 2013, **12**, 647-651.
7. F. He, T. Wu, R. Peng and C. Xia, *J. Power Sources*, 2009, **194**, 263-268.
8. H. Uchida, S. Tanaka and H. Iwahara, *J. Appl. Electrochem.*, 1985, **15**, 93-97.
9. L. Yang, Z. Liu, S. Z. Wang, Y. M. Choi, C. D. Zuo and M. L. Liu, *J. Power Sources*, 2010, **195**, 471-474.
10. Y. Choi, M. C. Lin and M. L. Liu, *Angew. Chem. Int. Edit.*, 2007, **46**, 7214-7219.
11. Y. M. Choi, D. S. Mebane, M. C. Lin and M. L. Liu, *Chem. Mater.*, 2007, **19**, 1690-1699.
12. M. M. Kuklja, E. A. Kotomin, R. Merkle, Y. A. Mastrikov and J. Maier, *Phys. Chem. Chem. Phys.*, 2013, **15**, 5443-5471.
13. Y. A. Mastrikov, R. Merkle, E. Heifets, E. A. Kotomin and J. Maier, *J. Phys. Chem. C*, 2010, **114**, 3017-3027.
14. Z. Wang, R. Peng, W. Zhang, X. Wu, C. Xia and Y. Lu, *J. Mater. Chem. A*, 2013, **1**, 12932.
15. G. Kresse and J. Furthmuller, *Comp. Mater. Sci.*, 1996, **6**, 15-50.
16. G. Kresse and J. Furthmuller, *Phys. Rev. B: Condens. Matter Mater. Phys.*, 1996, **54**, 11169-11186.
17. P. E. Blochl, *Phys. Rev. B: Condens. Matter Mater. Phys.*, 1994, **50**, 17953-17979.
18. J. P. Perdew, K. Burke and M. Ernzerhof, *Phys. Rev. Lett.*, 1996, **77**, 3865-3868.
19. H. J. Monkhorst and J. D. Pack, *Phys. Rev. B: Condens. Matter Mater. Phys.*, 1976, **13**, 5188-5192.
20. J. Goniakowski and C. Noguera, *Surf. Sci.*, 1996, **365**, L657-L662.
21. G. Henkelman and H. Jonsson, *J. Chem. Phys.*, 2000, **113**, 9978-9985.
22. E. Sanville, S. D. Kenny, R. Smith, and G. Henkelman, *J. Comp. Chem.*, 2007, **28**, 899-908.
23. W. Tang, E. Sanville, and G. Henkelman, *J. Phys.: Condens. Matter*, 2009, **21**, 084204.
24. S. L. Dudarev, G. A. Botton, S. Y. Savrasov, C. J. Humphreys and A. P. Sutton, *Phys. Rev. B: Condens. Matter Mater. Phys.*, 1998, **57**, 1505-1509.
25. Y. A. Mastrikov, R. Merkle, E. A. Kotomin, M. M. Kuklja and J. Maier, *Phys. Chem. Chem. Phys.*, 2013, **15**, 911-918.
26. L. Wang, T. Maxisch and G. Ceder, *Phys. Rev. B: Condens. Matter Mater. Phys.*, 2006, **73**, 195107.
27. G. Pilania, P. X. Gao, and R. Ramprasad, *J. Phys. Chem. C*, 2012, **116**, 26349-26357.
28. S. O. Choi, M. Penninger, C. H. Kim, W. F. Schneider, and L. T. Thompson, *ACS Catal.*, 2013, **3**, 2719-2728.
29. T. Ishigaki, S. Yamauchi, K. Kishio, J. Mizusaki and K. Fueki, *J. Solid State Chem.*, 1988, **73**, 179-187.
30. I. Ahmed, S. G. Eriksson, E. Ahlberg, C. S. Knee, M. Karlsson, A. Matic, D. Engberg and L. Borjesson, *Solid State Ionics*, 2006, **177**, 2357-2362.
31. P. G. Sundell, M. E. Björketun and G. Wahnström, *Phys. Rev. B: Condens. Matter Mater. Phys.*, 2006, **73**, 104112.
32. Y. Wang, M. Arai, T. Sasaki and C. Wang, *Appl. Phys. Lett.*, 2006, **88**, 091909.
33. A. Seidl, A. Görling, P. Vogl, J. A. Majewski and M. Levy, *Phys. Rev. B: Condens. Matter Mater. Phys.*, 1996, **53**, 3764-3774.
34. J. Robertson, *J. Vac. Sci. Technol. B*, 2000, **18**, 1785-1791.
35. Y. Rao, S. Zhong, F. He, Z. Wang, R. Peng and Y. Lu, *Int. J. Hydrogen Energ.*, 2012, **37**, 12522-12527.
36. B. He, Z. Wang, L. Zhao, X. Pan, X. Wu and C. Xia, *J. Power Sources*, 2013, **241**, 627-633.
37. K. D. Kreuer, *Chem. Mater.*, 1996, **8**, 610-641.
38. R. Hempelmann, M. Soertramo, O. Hartmann and R. Wappling, *Solid State Ionics*, 1998, **107**, 269-280.
39. M. S. Islam, P. R. Slater, J. R. Tolchard and T. Dinges, *Dalton T.*, 2004, 3061-3066.
40. S. J. Stokes and M. S. Islam, *J. Mater. Chem.*, 2010, **20**, 6258-6264.
41. E. Björketun, P. G. Sundell, G. Wahnström and D. Engberg, *Solid State Ionics*, 2005, **176**, 3035-3040.
42. M. A. Gomez, M. A. Griffin, S. Jindal, K. D. Rule, and V. R. Coope, *J. Chem. Phys.*, 2005, **123**, 094703.
43. W. Münch, K.-D. Kreuer, G. Seifert, and J. Maier, *Solid State Ionics*, 2000, **136-137**, 183-189.
44. P. I. Dahl, H. L. Lein, Y. Yu, J. Tolchard, T. Grande, M.-A. Einarsrud, C. Kjølseth, T. Norby and R. Haugrud, *Solid State Ionics*, 2011, **182**, 32-40.
45. K. Momma and F. Izumi, *J. Appl. Crystallogr.*, 2011, **44**, 1272-1276.

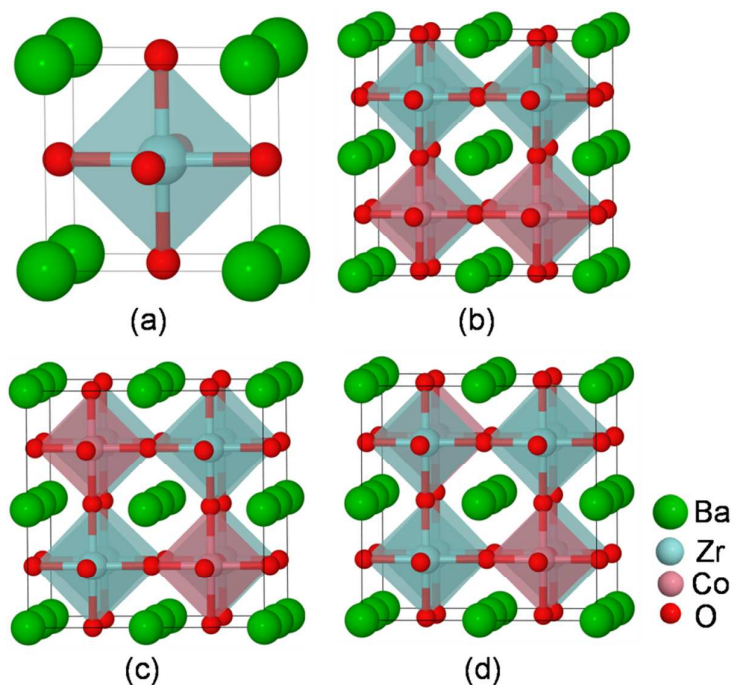


Fig. 1 (a) The cubic unit cell structure of BaZrO₃ and (b)-(d) three possible Co atom arrangements of BaZr_{0.75}Co_{0.25}O₃ in a 2x2x2 supercell.

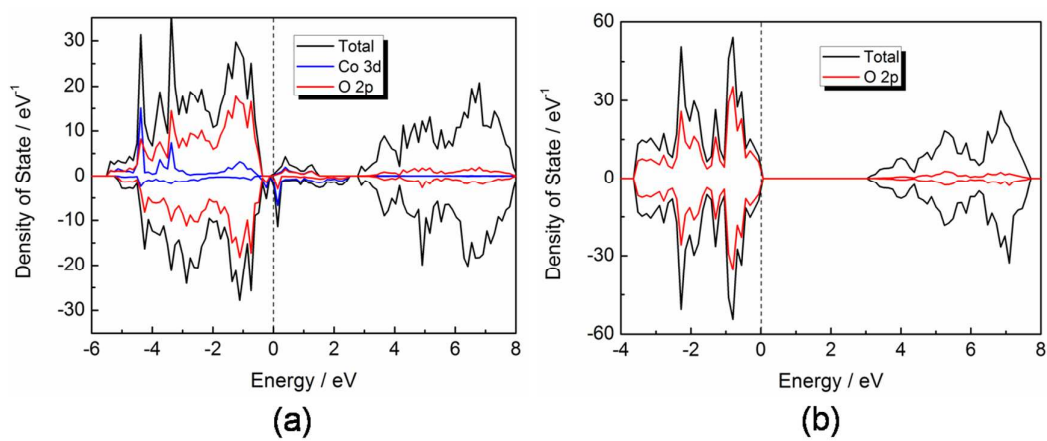


Fig.2 Density of State of (a) BaZr_{0.75}Co_{0.25}O₃ and (b) BaZrO₃, respectively.

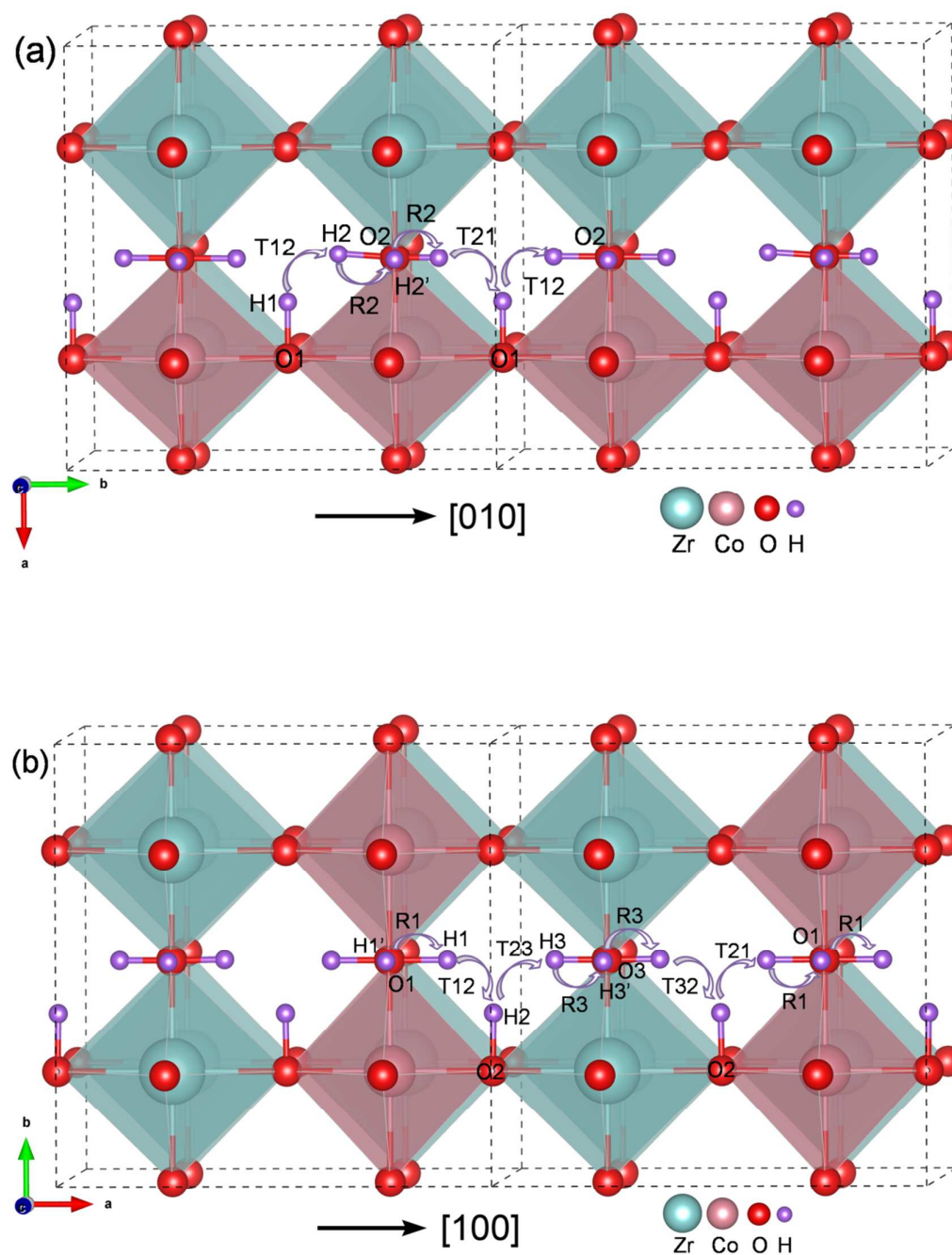


Fig 3. Schematic representations of the proton transporting along (a) [010] and (b) [100] directions. On ($n=1, 2, 3$) denotes different oxygen position. R and T refer to proton rotation and transferring. For example, R1 refer to proton rotating along the O1, and T12 refer to proton transferring between O1 and O2. Moreover, $H_n(n=1, 2, 3)@O(n=1, 2, 3)$ stands for the possible proton locations.

Table 1a. Energy barriers of proton migration along the pathway [010] direction and relative structure energies.

[010]	T12	R2	R2	T21
Barriers / eV	0.53	0.05	0.22	0.03
H-sites	H1@O1	H2@O2	H2'@O2	
$\Delta E_{\text{site}} / \text{eV}$	0	0.42	0.24	

Table 1b. Energy barriers of proton migration along the pathway [100] direction and relative structure energies.

[100]	R1	T12	T23	R3	R3	T32	T21	R1
Barriers / eV	0.05	0.53	0.63	0.01	0.26	0.17	0.03	0.05
H-sites	H1'@O1	H1@O1	H2@O2	H3@O3	H3'@O3			
$\Delta E_{\text{site}} / \text{eV}$	0	0	0.42	0.93	0.69			

Here, Hn(n=1,2,3)@O(n=1,2,3) denotes the possible proton locations. ΔE_{site} , the relative structure energy, is defined as the energy difference between the most stable proton incorporation site (H@O1) and possible proton locations.

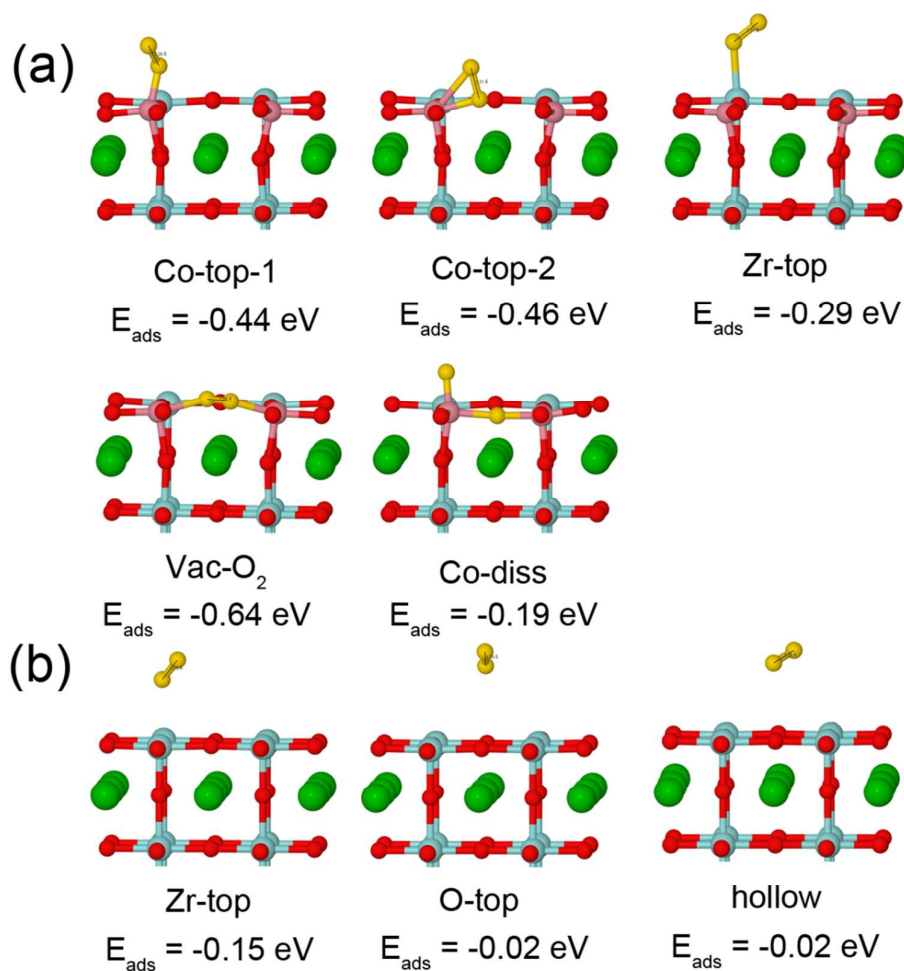


Fig. 4 The optimized O₂ adsorption structures on (a) the CoO-terminated BaZr_{0.75}Co_{0.25}O₃ (100) surface and (b) the BaZrO₃ (100) surface. E_{ads} refers to the estimated oxygen adsorption energy, which is defined as $E_{\text{ads}} = E[\text{slab} + \text{O}_2] - E[\text{slab}] - E[\text{O}_2]$. The golden atom denotes an oxygen from the O₂ molecule.

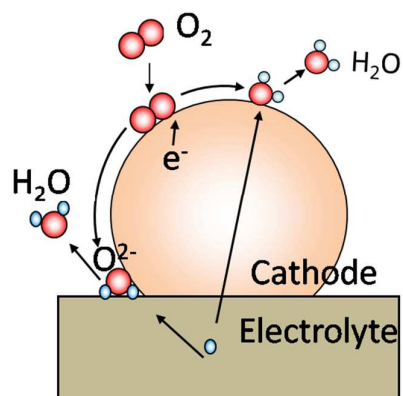
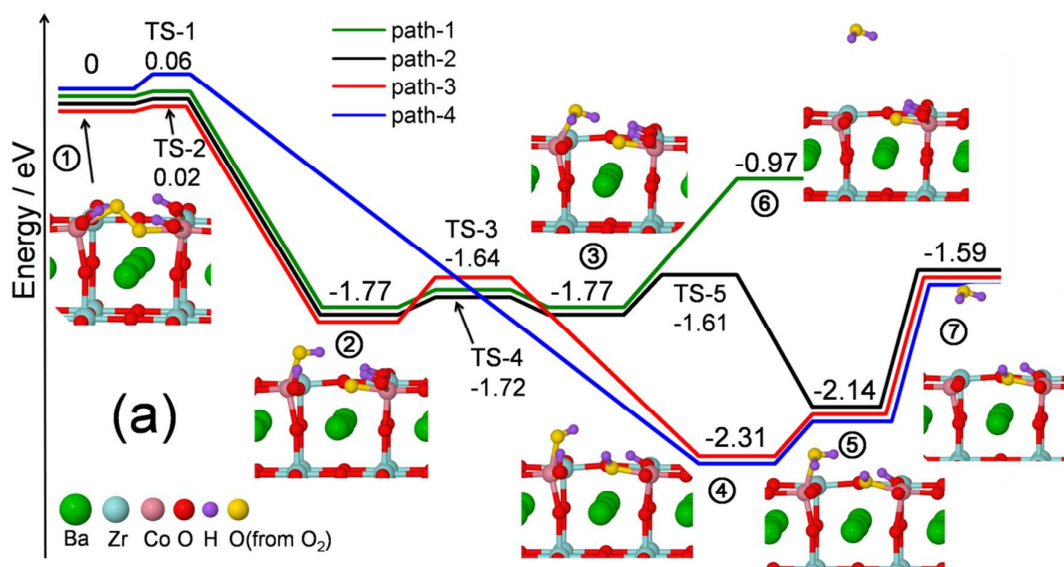


Fig. 5 Schematic diagram of the possible reaction at the mixed protonic/electronic cathode materials (e.g. BZCO) in H-SOFCs.



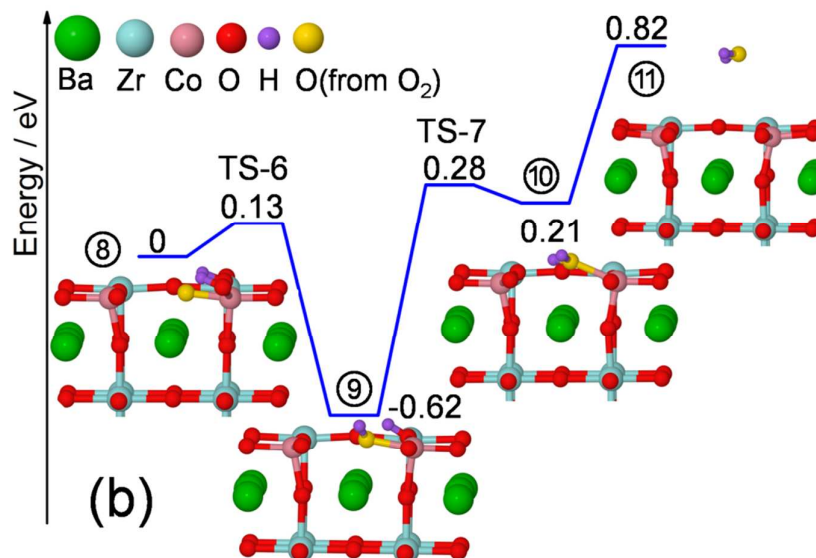


Fig. 6 Potential energy diagram for oxygen reduction on the BZCO (100) cathode surface. (a) four plausible reaction pathways of the adsorbed O₂ molecule forming the first water. (b) the reaction pathway producing the second water. Numbers in Circle denote the structure name.